SLAC-PUB-2882
February 1982
(E/I)

ENERGY LOSS MEASUREMENT IN A JET CHAMBER*

J. Va'vra, L. Roberts, D. Freytag and P. Clancey
Stanford Linear Accelerator Center
Stanford University, Stanford, California 94305

ABSTRACT

A full size prototype cell of a multiwire detector similar in design to the JADE [2] drift cell geometry was tested in a beam of pions and electrons at SLAC. The motivation was to explore the possibility of identifying particles through a measurement of energy loss in the HRS experiment [1]. The purpose of the test was to investigate the extent of which the measurement of the energy loss is degraded as one makes the transition from a small chamber to a full size detector. We also measured the reduction in gas gain due to saturation effects as a function of the track angles relative to the chamber wires and as a function of the total gain in the chamber.

We compared our results and data reported by other groups with an empirical model calculation for the energy loss as a function of various parameters.

We also developed a program to calculate expected pulse shapes for different chamber geometries. This program [10] simulates the drift process of randomly generated clusters of ionization in the electrostatic field defined by the chamber parameters. The results of this calculation are essential to evaluate the multiple hit capability of the jet chamber and its dependence on the design parameters.

(Submitted to Nuclear Instruments and Methods)

* Work supported by the Department of Energy, contract DE-AC03-76SF00515.

INTRODUCTION

Our motivation was to design the detector for the π/e identification below 4 GeV/c and particle identification in the $1/\beta^2$ region of the dE/dx curve. Since we were considering the possibility of using the prototype in the HRS magnet we had to meet several constraints for the construction of the chamber.

(a) The available space limited the total radial extent of the dE/dx detector to about 70 cm.

(b) We decided not to instrument the tracking electronics in the prototype, since the HRS spectrometer already has the tracking chambers.

(c) No measurement of the coordinate along the wire by charge division was attempted. Thus only small capacitors were needed to couple to the sense wires, which were at positive potential. The side electrodes were at ground potential, which considerably simplified the construction problems.

(d) The large size of a final dE/dx detector required a strong and lightweight modular construction. We decided to use Hexel panels in the construction of the body of the prototype.

(e) Because of very difficult access to the magnet we placed the amplifiers at a distance of 15 ft from the chamber. The cable introduced noise into the system and prevented us from operating the chamber with a gain as low as 10^3 where one does not have angular corrections introduced by the saturation effects.

(f) The allowed space for the detector starts at 1.1 m from the interaction point where multiple tracks are already separated. It was therefore decided that the single hit analog electronics would be sufficient for the HRS application.

In addition to the above specific motivation, we were interested in investigating the jet chamber concept in general. The main strength of this particular geometry of a drift cell is a uniform electric field which is advantageous for resolving multiple tracks. This concept was pioneered by the JADE [2] and AFS [3] detectors. They used charge division, which generally forces one to run the chamber at higher gain. As a result, one has to deal with angular corrections which are poorly known. Therefore, we decided to measure the corrections for several gains.

Finally, we compared our results with predictions derived from a simple phenomenological model which uses measured data for energy loss as input. It is based on work of Walenta [5] and Allison [4] with additions by us.

DESCRIPTION OF THE PROTOTYPE

The dimensions of the drift cell are shown on fig. 1. The drift chamber body was constructed using hexel panels as shown on fig. 2. The construction technique was modular, based on the use of flat hexel panels. The hexel panels were made on a precision granite table to ensure the flatness of the bottom side. The top side was held down by evacuating a volume confined by a mylar sheet sealed around the edges by zinc chromate tape sealant. The precision in flatness of the top was determined by the tolerance on thickness of the aluminum hexel core. The total variation in the thickness of the panel was measured to be less than ±50 μm. The hexel core and the aluminum skins were glued together using HYSOL EA9410 glue. It was found to be important that

the individual hexel core cells were connected to each other through small pinholes, in order to apply a negative pressure uniformly across the whole panel. The panels were covered by a Styrofoam sheet during the drying period to ensure good temperature uniformity. As one can see, we have used a "cold technique" to produce the hexel panels. For mass production we would use Hexabond, which is a hexel core with bonding adhesive already applied and which cures at 260°C.

Imbedded in the central hexel panel was a movable rod holding Fe^{55} and Cd^{109} x-ray sources deposited every 1.2 cm (fig. 3). The rod could be moved back and forth by applying a small gas pressure. In the open position the x-rays could penetrate the square brass tubing through a series of small holes and enter the chamber through a 100 μm aluminum foil. The activity in each source dot was 200 μCurie for Fe^{55} and 50 μCurie for Cd^{109}. This system was essential for correcting the shifts in gas gain during the test.

The finished hexel panels were glued together, using a precision jig. It is important to note that mechanical dimensions have to be tightly controlled. From our previous study [6] we determined that for the desired tolerance in gain of ±1% we had to keep the cathode flat to about ±0.1 mm. In particular, we tried to avoid systematic departures from flatness. The hexel panels were held at the ends by LEXAN flanges which also had feed-throughs for the wires. The whole chamber was a lightweight and mechanically very rigid system. Due to the finite width of the side hexel panels, the chamber had about 8% of dead space. The chamber can be seen in fig. 4.

The advantage of this design is that the cell has a small number of wires, the cathode plane is perfectly flat and the cell does not have any boundaries because of supporting members such as JADE.

The total active length of the chamber was 225 cm. The 37.5 μm diameter gold-plated tungsten sense wires were tensioned to 153 grams, the 100 μm diameter beryllium-copper field wires were tensioned to 407 grams in order to obtain the same gravitational deflection as for the sense wires. The field wires at the ends of the chamber were made of 150 μm diameter beryllium-copper wire. The wires were held in the Delrin pins using a crimping technique. We used the crimping tool SP-02 Squeeze-Eze made by Simonds Machine Co., Massachusetts. To ensure that the side hexel panels were not bowed due to gas over-pressure, we enclosed the prototype in an envelope made of Kapton foil.

The wires were run at positive voltages and the aluminum hexel panels at ground. We used single hit analog electronics available at SLAC with some modifications. Each sense wire was connected through the high voltage decoupling capacitor (500 pf) and 15 ft of twisted pair cable into the charge integrating amplifier [7] operating with ~50 μsec RC decay constant. The resulting pulse was strobed by a 100 ns gate into an analog sample and hold module SHAM IV [8] . The sampling gate arrived about 2 μsec after the avalanche was formed. The stored analog data were then scanned and digitized to 12-bit accuracy using the BADC [9] with subsequent transfer to an LSI-11 computer. The σ noise was typically 2.8×10^4 electrons referred to the amplifier input when compared with the most probable signal value of 1.1×10^6 electrons at the chamber gas gain of about 2×10^4. The largest contributor to the noise was the ~15 ft long cable in front of the amplifier.

DESCRIPTION OF THE TEST SETUP

The test was performed in the SLAC Test Beam Facility. The data were taken at 4 GeV/c by alternating between pion and electron beams. At this momentum, one expects the relativistic rise to be about 31% in 90% argon + 9% CO_2 + 1% CH_4 gas. Our measured relativistic rise is 26.4% at a gain of 2×10^4. The selection of a particle was done using a differential Cerenkov counter and by the insertion of a lead sheet to suppress the electron background in case of the pion beam. The beam size was about 5 mm FWHM. Two small coincidence counters in front and behind insured that the beam passed through the chamber. The suppression of events with two or more particles per SLAC pulse was done off-line by rejecting doubles in a pile-up gate and fast scaler coupled to the beam defining counter.

The stability of the electronics and the gas gain was monitored by using the Fe^{55} source rod before and after every run, lasting typically one hour. The chamber was mounted on a table which allowed easy adjustment in the vertical and horizontal directions, as well as rotations in the two angles θ and ψ which are defined in fig. 7.

DESCRIPTION OF THE RESULTS

(a) Analysis of the Data

After the pedestal subtraction the individual measured pulse heights were corrected for the cross-talk using the matrix correction:

$$\left.\frac{dE}{dx}\right|_{\text{TRUE}} = A^{-1} \left.\frac{dE}{dx}\right|_{\text{MEASURED}}$$

where $a_{i,i} = 1.0$, $a_{i,i\pm1} = -0.056$, $a_{i,i\pm2} = -0.019$, $a_{i,i\pm3} = -0.007$, other $a_{ik} = 0$. These values were obtained from the electrostatic program [10]

by applying an incremental voltage to a given sense wire and obtaining the relative changes of the charges on neighboring wires compared to their nominal values. These calculated values were found to be in good agreement with the measurements [6]. The correction increased the average pulse height by ~28% and improved the corrected resolution of the energy loss measurement from σ/peak = 9.8% to 9.3% (π's, $\theta = 0^{o}$, 36 samples, 1.2 cm/sample). The π/e separation was improved on the average by 3% to 4% by applying the cross-talk correction, i.e., a rather small improvement. However, this effect becomes more severe if the cross-talk between wires is increased, which we have done in a model calculation based on our data. For 14% cross-talk, the particle separation would be reduced by more than 30% and for 17% cross-talk by a factor of 2. In practice we would try, of course, to correct the data, but the question remains how accurately this can be done. Our conclusion is that one should not allow cross-talk to be larger than 10-12%.

In the next step the data were corrected for gain variations between the individual wires as determined in the π beam. The typical necessary adjustment was less than 10%. The next step was to plot the truncated mean distributions, where we rejected about 30% of the largest pulse height values. At this point we corrected for the overall gain shift as a function of time using the Fe^{55} calibration runs. Typically, this correction was less than 1.5%. The truncated mean distributions were then fitted with a Gaussian curve. Figures 5 and 6 show two examples of such fits, one for the beam going perpendicularly to the wires ($\theta = 0^{o}$) and one for $\theta = 45^{o}$.

(b) Saturation Corrections as a Function of Track Angles

The saturation effect is one of the most serious corrections if one wants to combine dE/dx data for different θ's and ψ's (see fig. 7 for definitions of these angles). The effect is caused by a modification of the electric field by the presence of the positive ions from the first avalanche and its influence on the amplification of the next avalanche hitting the same spot of the wire. This becomes noticeable above a gain of about 5×10^3 and is particularly important in the jet chamber if charge division is used, necessitating higher gains (typically 5×10^4 or more). We believe that the magnitude of the saturation correction depends on the diameter of the sense wire, a larger wire diameter yielding a smaller correction. Diffusion of the drifting charge should also affect the saturation, although we do not have direct evidence in our data.

We have measured saturation corrections for various gains in the chamber. First, we wanted to ensure that we did not have a dependency on the position of the beam in the chamber. We made scans of pulse height as functions of x and z and we found the maximum variation of pulse height to be less than 1%. Figures 8 and 9 show the θ and ψ angle dependencies for various gains in the chamber. We can see that the pulse height is very sensitive to the angle θ. As we change the angle we tend to populate regions along the wire still free of positive ions. Thus the mean pulse height increases with θ. This does not happen when we vary the ψ angle. In this case the same region of the wire is populated by the arriving charge clusters.

However, there are other systematic effects apart from the saturation which can affect the angular dependence of the pulse height measurement.

For instance a finite integration time can reduce the pulse height at large ψ angles, especially in the presence of the large magnetic field, see Fig. 11f. Also, the biasing of the field wires must be done carefully to minimize the pulse height changes at small ψ angles. [6]

(c) Multiple Tracks in the Chamber

We did not have appropriate electronics to study the problem of multiple tracks in detail. Nevertheless, fig. 10 clearly indicates our ability to recognize mutliple hits in the chamber using the dE/dx measurement.

We have decided to study the problem of multiple hits theoretically. We have developed a program which combines a regular electrostatic program [10] with a section following the drifting of the charge clusters in an accurate electric field. The propagation of the charge is performed in small steps and in each step the program modifies the drift trajectory including the diffusion and the Lorentz angle. The final drift time distribution can then be convoluted with the effects of avalanche formation and the response of the amplifier and appropriate filters. Figures 11(a)-(i) show predicted drift time distribution for parallel tracks of fixed separation in our prototype cell. One can see that the drifting charge has a considerable tail even before the amplification process, especially for some track orientations in large magnetic fields. In order to reduce the overall length of this tail one has to reduce the wire spacing as, for instance, the AFS [3] detector did. Another possibility is to run the field wires between the sense wires at such a voltage that they collect some of the charge thus reducing the sample size collected on the sense wire. Figure 11(i) indicates the drift time distributions

for running the field wires at the same potential as the sense wires, i.e., making the effective sample size about half of the original. The improvement in the charge collection time is obvious. The penalty for this approach is higher voltages in the cell to obtain the necessary gain. Another disadvantage is a degradation of the dE/dx performance because the total effective length of the chamber is half of the original.

To illustrate a possible limit in the jet chamber design, fig. 11(j) shows an example of 1 mm spacing between the sense and field wires for a case of two tracks 500 μm apart in a slow gas (we took as an example 90% argon + 10% methane). Figure 11(k) shows the result of a convolution of the drift distributions from fig. 11(j), a $1/[1+(t/t_o)]$ tail due to positive ions ($t_o \cong 0.3$ ns for ϕ 10 μ sense wires), two zero pole filters canceling this tail, ~2 ns rise time of the preamplifier and the Gaussian integrator with FWHM ≅ 8 ns according to R. A. Boie [24]. In this example we assume that the field wires are running at +500 volts in order to collect the charge and reduce the effective sample width on the sense wire to about 500 μm.

COMPARISON WITH AN EMPIRICAL MODEL FOR ENERGY LOSS CALCULATION

There are various theoretical methods used to predict the particle separation using the dE/dx technique [4],[11],[12],[13]. We have decided to use a phenomenological approach based on experimental data. While this approach is not theoretically the most elegant, nevertheless it is quite simple and it provides a quick prediction for various possible configurations. The important thing is that all experimental input comes from the single cell data, because the large experiments very likely have various systematic errors, which degrade the performance.

We want to determine the dE/dx separation in units of standard deviations:

$$\frac{\Delta E}{\sigma} = \frac{E_2 - E_1}{\sigma(n)} = 2.35 \times \frac{E_2 - E_1}{E_1} \times \frac{E_1}{W(n)} \qquad (1)$$

where

n - total number of samples

E - the most probable energy loss

W(n) - FWHM for n samples

$\sigma(n)$ - standard deviation for n samples.

The n dependence was measured by several experiments [6],[16],[17].

$$\frac{\Delta E}{\sigma} = 2.35\, n^{0.43} \times \frac{E_2 - E_1}{E_1} \times \frac{E_1}{W(n)} \qquad (2)$$

where

W(1) - FWHM for one sample

E_1 - is taken to be the heavier particle.

We assume that the most probable energy loss is given by the following formula [14],[15]:

$$E = \frac{\alpha t}{\beta^2}\left[\underbrace{\ln \frac{m_e c^2 \alpha t}{I^2} + 0.891}_{k} + 2 \ln \beta\gamma - \ln \beta^2 - \beta^2 - \delta\right] \qquad (3)$$

where

k - a term containing the properties of the gas

I - mean ionization potential

αt - $0.153(z/A)t$ (MeV for t in g/cm^2)

δ - density correction term.

Walenta [5] determined the density term from eq. (3) by measuring ratios of E/E_{min} for various gases, pressures, and momenta in the single cell detector.

At this point we extend his work. The aim is to find a convenient parameterization of the density term so we can predict the energy loss for any gas and pressure. We have replotted his density data as a function of log γ and fitted the data for various k_1 constants using the following function:

$$\delta = a(k_1) + b(k_1) \log \gamma + c(k_1)(\log \gamma)^2 \qquad (4)$$

where

$$k_1 = k - \ell n\ (t/t_1) \quad , \quad t_1 = 1 \text{ cm} \quad .$$

The fit was constrained by demanding that the density function asymptotically approach 2 $\ell n\ \beta\gamma$, as is required if we want to cancel the relativistic rise of the energy loss — see eq. (3). Table I gives the list of parameters from eq. (4) for various k_1 constants. We used linear interpolation in between various k_1 fits. Now we can predict $(E_2 - E_1)/E_1$ function in eq. (2) for any gas and pressure as a function of momentum.

The next quantity to determine is $E_1/W(1)$ in eq. (2). We will use Allison's [4] fit to Walenta's single cell data [5]:

$$\frac{W(1)}{E} = 81.0 \left(\frac{\alpha t}{I}\right)^{-0.32} \quad . \qquad (5)$$

Now we have all equations necessary to predict the particle separation by energy loss for various experiments. Table II shows comparisons between measured results from this experiment as well as some other major tests, and our prediction from the simple empirical model. One can see that most of the large tests are worse by 10-30% compared to our simple model, presumably due to various systematic problems.

The table shows the relative quantity $\Delta E/\sigma$ as well as an absolute measure of the resolution σ/E. We prefer the comparison with the relative quantity $\Delta E/\sigma$.

Figures 12, 13 and 14 show various predictions of our simple model as a function of number of samples, pressure and gases.

CONCLUSIONS

We have measured the energy loss in the jet chamber for π's and e's at 4 GeV/c. The comparison with a simple phenomenological model indicates a reasonable agreement within 20%. We have also mapped the angular saturation corrections as a function of several gains in the chamber. The knowledge of these corrections is necessary if one operates the jet chamber at gains higher than 5×10^3. The limited dE/dx measurement can be useful to resolve TOF ambiguities in the $1/\beta^2$ region of the energy loss curve and to determine the multiplicity of the charged tracks in the core of the jets.

ACKNOWLEDGEMENTS

We would like to thank Dr. L. Keller for his support and interest in this project. Also, a number of suggestions from H. W. Weidner and T. Pulliam were appreciated. We would like to thank Jack Nicol, M. Starek, Dianne Chamberlin, Bryan Harris, and Dorothy Edminster for excellent technical support.

REFERENCES

[1] HRS Proposal, PEP-12.

[2] W. Farr et al., Nucl. Instrum. Methods 156 (1978) 283.
W. Farr and J. Heintze, Nucl. Instrum. Methods 156 (1978) 301.
H. Drumm et al., Nucl. Instrum. Methods 176 (1980) 333.

[3] D. Cockerill et al., Nucl. Instrum. Methods 176 (1980) 159.
O. Botner et al., CERN/EF/0424H/HJH/ed, 1981.
J. C. Berset et al., Nucl. Instrum. Methods 176 (1980) 251.

[4] W. W. M. Allison and J. H. Cobb, Oxford University Pub., Ref. 12/80.

[5] A. H. Walenta, BNL Report, BNL-28328, 1980.

[6] J. Va'vra and D. Rust, SLAC-PUB-2635, 1980.

[7] D. Freytag, SLAC-PUB-2622, 1980.

[8] E. Cisneros et al., SLAC-PUB-2641, 1980.

[9] M. Breidenbach et al., SLAC-PUB-2032, 1977.

[10] To be published. For more details on various possible designs see our SLAC SLC Notes No. 31 and No. 60.

[11] R. Talman, Nucl. Instrum. Methods 159 (1979) 189.

[12] D. Ritson, SLAC Summer School (1980).

[13] G. Lynch, LBL Physics Notes, TPC-LBL-81-6.

[14] L. Landau, J. Phys. USSR 8 (44) 201.

[15] R. Sternheimer, Phys. Rev. D3 (1971) 3681.

[16] A. H. Walenta, Nucl. Instrum. Methods 161 (1979) 45.

[17] Aderholz et al., Nucl. Instrum. Methods 118 (1977) 419.

[18] D. Fancher et al., Nucl. Instrum. Methods 161 (1979) 383.

[19] W. W. M. Allison et al., Nucl. Instrum. Methods 163 (1979) 331.

[20] B. F. Wadsworth et al., IEEE Trans. Nucl. Sci. NS-26 (1979).

[21] I. Lehraus et al., Nucl. Instrum. Methods 153 (1978) 347.

[22] R. Ehrlich et al., CBX 80-43, 1980.

[23] I. Lehraus et al., CERN/EF 81-14, 1981 and CERN/EF 82-1, 1982.

[24] R. A. Boie et al., IEEE Trans. Nucl. Sci. NS-28 (1981) 603.

[25] A. Wagner, Proceedings from 1982 SLAC Instrumentation Conference.

TABLE I

k_1	$a(k_1)$	$b(k_1)$	$c(k_1)$	Condition
6	+10.065	-8.5619	1.82804	$\log(\gamma) \leq 3.6$
	-13.63	4.6	0.0	> 3.6
7	+ 4.1334	-4.5857	1.27579	$\log(\gamma) \leq 3.6$
	-12.4	4.6	0.0	> 3.6
8	+ 0.8135	-2.1447	0.93676	$\log(\gamma) \leq 3.6$
	-11.33	4.6	0.0	> 3.6
9	0.00402	-1.1582	0.79975	$\log(\gamma) \leq 3.0$
	-10.36	4.6	0.0	> 3.0
10	- 1.7564	0.67256	0.49093	$\log(\gamma) \leq 3.0$
	- 9.611	4.6	0.0	> 3.0
11	- 1.5065	1.0156	0.44805	$\log(\gamma) \leq 3.0$
	- 8.6753	4.6	0.0	> 3.0

TABLE II

DEVICE	n.t.P cm. atm	PARTICLE	P GeV/c	$\frac{\Delta E}{\sigma}$ exp	$\frac{\Delta E}{\sigma}$ model	$\frac{\sigma}{E}$ exp	$\frac{\sigma}{E}$ model	COMMENT
TPC(T) [18]	192 × 0.4 × 10	π/e	0.8	11.8	14.8	2.7%	2.8%	80% Argon + 20% CH_4
ISIS(T) [19]	60 × 1.6 × 1	π/e	0.5	8.0	10.9	6.0	6.1	80% Argon + 20% CO_2
CRISIS(T) [20]	64 × 1.5 × 1	p/π	40.0	2.2	2.8	6.0	6.0	80% Argon + 20% CO_2
EPI [21]	128 × 6.1 × 1	p/π	50.0	5.1	4.8	2.8	2.9	95% Argon + 5% CH_4
JADE [2]	48 × 1 × 4	π/e	0.45	8.1	10.1	5.9	5.0	Resolution taken from Bhabha events with more than 42 good samples
JADE [2]	48 × 1 × 4	π/e	0.45	4.2	10.1	8.5-10.2	5.0	Jet Events
JADE [25]	45 × 1 × 4	e^-	2.0	--	--	4.9	5.1	Test beam results
CLEO [22]	117 × 0.667 × 3.0	π/e	1.0	8.2	11.5	5.0	4.2	91% Argon + 9% CH_4
LEHRAUS [23] DRIFT	64 × 4 × 1	π/e π/p	15.0	3.00 5.29	3.4 4.9	4.7	4.4	95% Argon + 5% CH_4
- " -	64 × 4 × 5	π/e π/p	15.0	3.01 5.98	3.2 6.6	3.0	2.6	
- " -	64 × 4 × 1	π/e π/p	15.0	1.84 4.35	2.6 5.4	4.4	3.8	50% Argon + 50% C_2H_6
- " -	64 × 4 × 4	π/e π/p	15.0	1.60 3.48	2.7 5.4	3.5	2.5	
THIS TEST $\theta = 0^o$	36 × 1.2 × 1	π/e	4.0	2.9	3.7	9.3	8.3	90% Argon + 9% CO_2 1% CH_4
THIS TEST $\theta = 45^o$	$36 \times \frac{1.2}{\cos 45^o} \times 1$	π/e	4.0	3.4	4.1	8.1	7.4	

FIGURE CAPTIONS

1. Dimensions of the drift cell. Two such cells for prototype.
2. Schematic description of the construction of the prototype using Hexel panels.
3. Method of instrumenting the Fe^{55} and Cd^{109} x-ray sources in the central Hexel panel.
4. Overall view of the finished prototype.
5. Truncated mean distributions for π's and e's at 4 GeV/c for $\theta = 0^{o}$, $\psi = 0^{o}$, 36 samples used, 1.2 cm/sample, cross-talk correction in, total gain $\sim 2 \times 10^{4}$, 10 largest out of 36 rejected.
6. Truncated mean distributions for π's and e's at 4 GeV/c for $\theta = 45^{o}$, $\psi = 0^{o}$, conditions as in fig. 5 except sample size is 1.2 cm/cos 45^{o}.
7. Definitions of ψ and θ angles, and x,y,z coordinate system.
8. Saturation corrections as a function of θ angle for various gains in the chamber.
9. Saturation corrections as a function of ψ angle for various gains in the chamber.
10. Multiple hit separation in the prototype for 4 GeV/c e^{-}, 35 samples, no cross-talk correction.
11. (a)-(h) Drift time distributions of individual charge clusters in this prototype for various conditions.

    (i) $\psi = 0^{o}$, $B = 0^{o}$, one track, field and sense wires at the same potential, this prototype (to be compared with 11(a) distribution).

    (j) $\psi = 0^{o}$, B = 5 kG, pressure 30 atm, 1 mm spacing between the sense and field wires, the field wire potential +500 volts (possible design).

(k) Convolute the fig. 12(j) with $1/[1+(t/t_o)]$ tail due to positive ions, two zero pole filters to cancel it, 2 ns rise time due to preamplifier and the Gaussian integrator with FWHM $\cong$ 8 ns to symmetrize the pulse shape [24].

12. Particle separation $\Delta E/\sigma$ in number of standard deviations as a function of pressure for 90% Argon + 10% CH_4, 0.4 cm/sample and n = 200 samples.

13. Particle separation $\Delta E/\sigma$ in number of standard deviations as a function of number of samples for 90% Argon + 10% CH_4, 1.0 cm/sample and pressure 1.0 atm.

14. Particle separation $\Delta E/\sigma$ in number of standard deviations as a function of gas for 1.0 cm/sample, pressure 1.0 atm and n = 40 samples. A modest gain can be seen in $1/\beta^2$ region for gases with lower mean ionization potential.

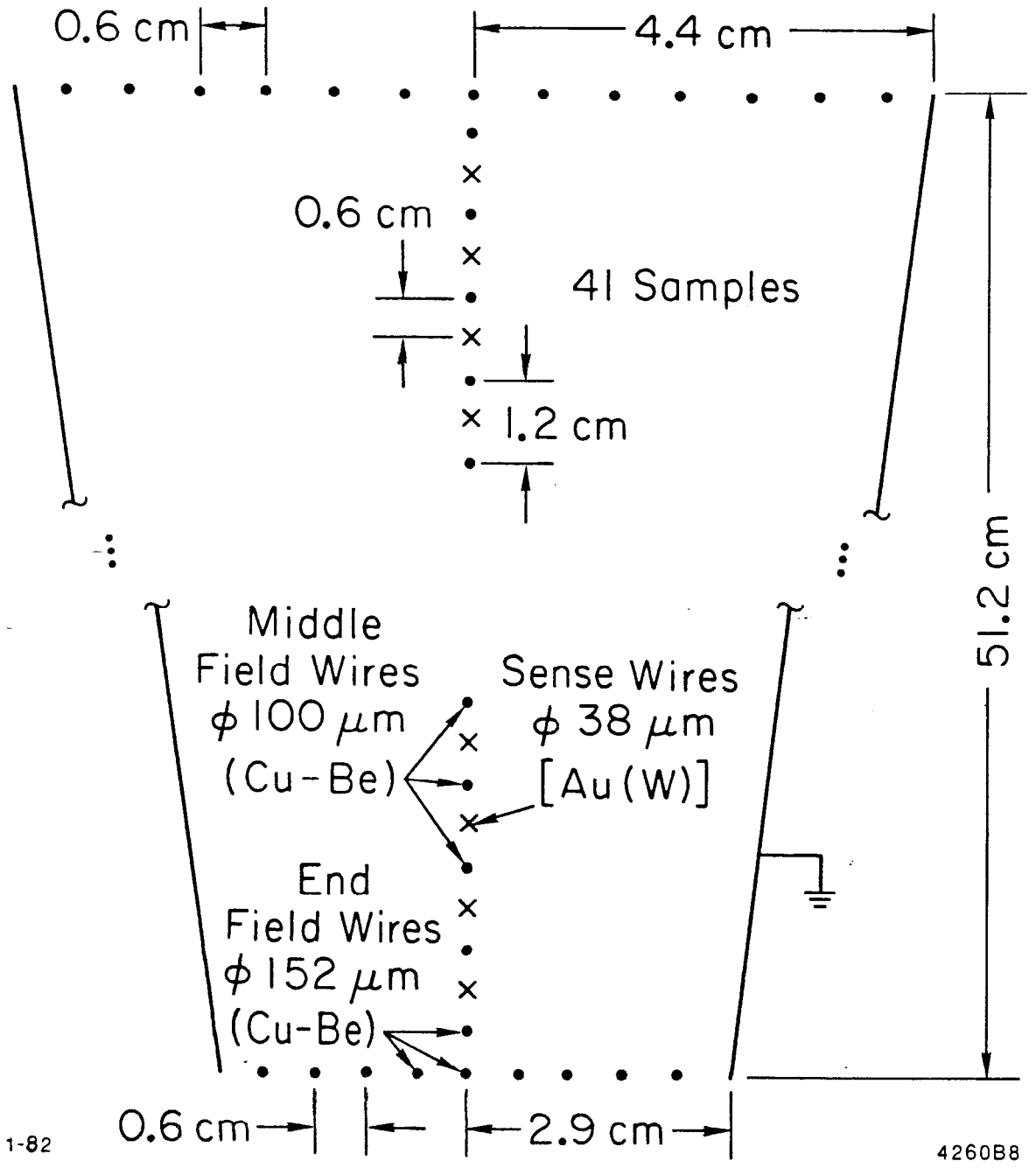
0.6 cm
4.4 cm
0.6 cm
41 Samples
1.2 cm
51.2 cm
Middle
Field Wires
φ 100 μm
(Cu-Be)
Sense Wires
φ 38 μm
[Au(W)]
End
Field Wires
φ 152 μm
(Cu-Be)
0.6 cm
2.9 cm
1-82
4260B8

Fig. 1

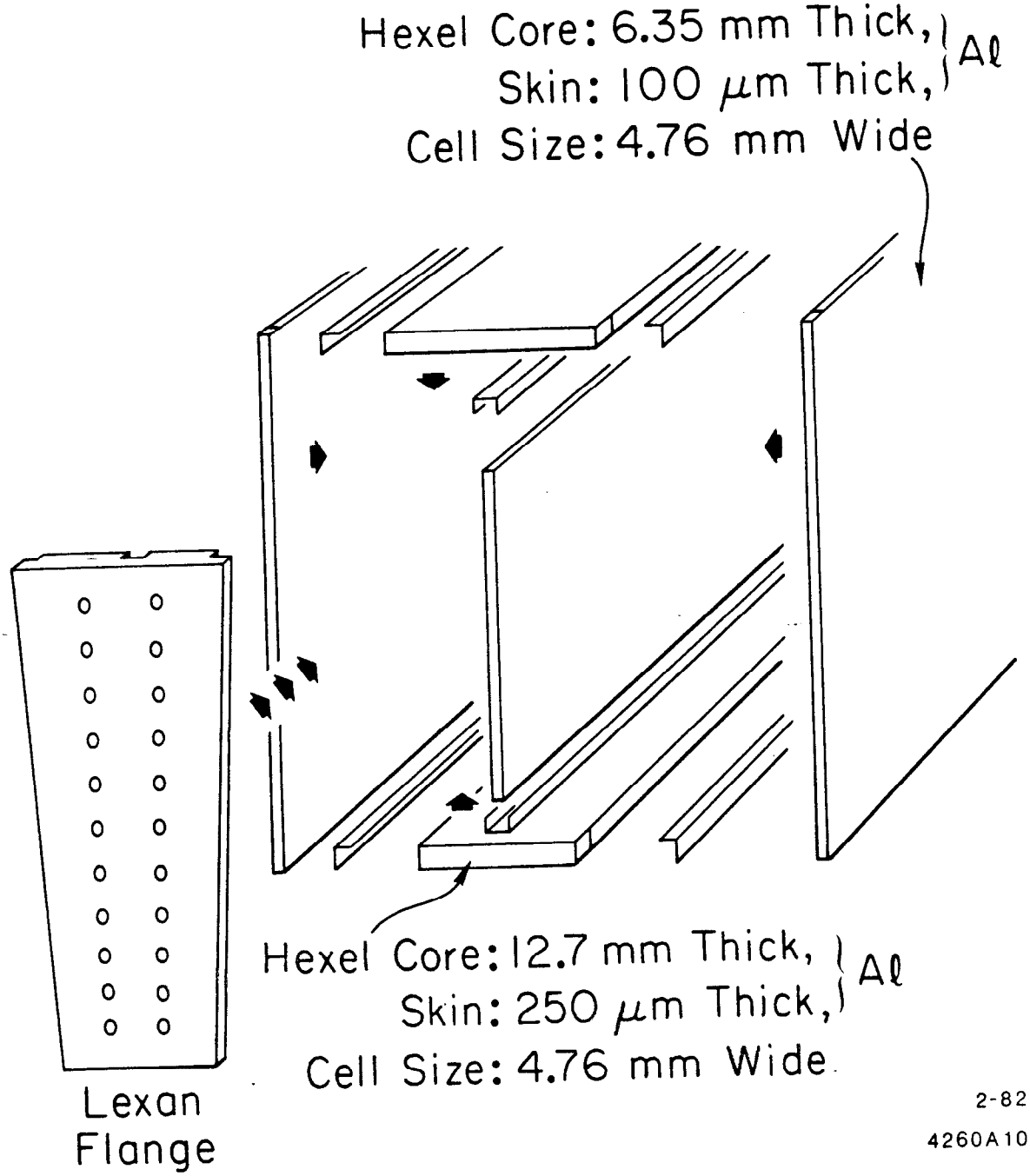
Hexel Core: 6.35 mm Thick,
Skin: 100 μm Thick,
Al
Cell Size: 4.76 mm Wide
Hexel Core: 12.7 mm Thick,
Skin: 250 μm Thick,
Al
Cell Size: 4.76 mm Wide
Lexan
Flange
2-82
4260A10

Fig. 2

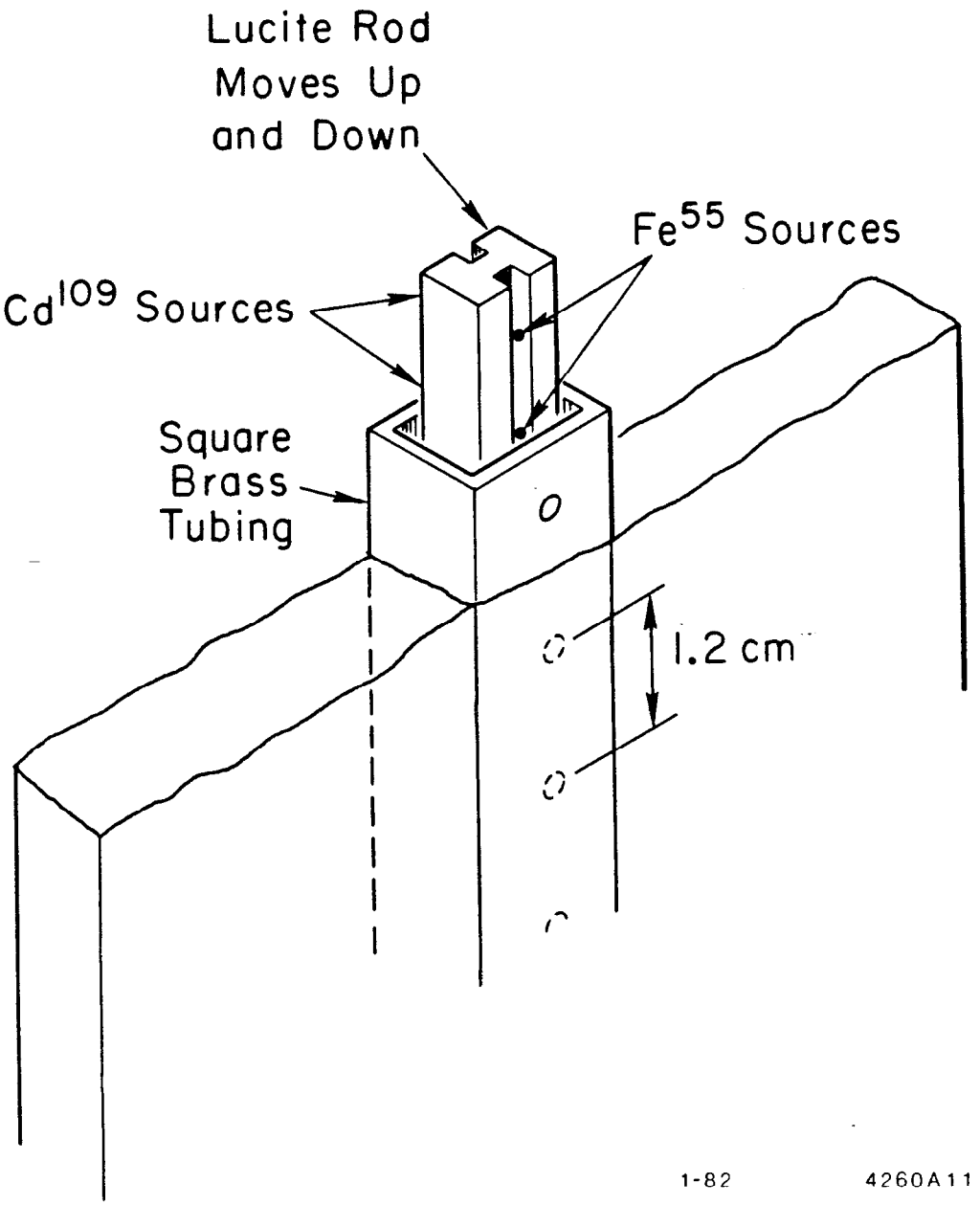
Lucite Rod
Moves Up
and Down
Fe55 Sources
Cd109 Sources
Square
Brass
Tubing
1.2 cm
1-82
4260A11

Fig. 3

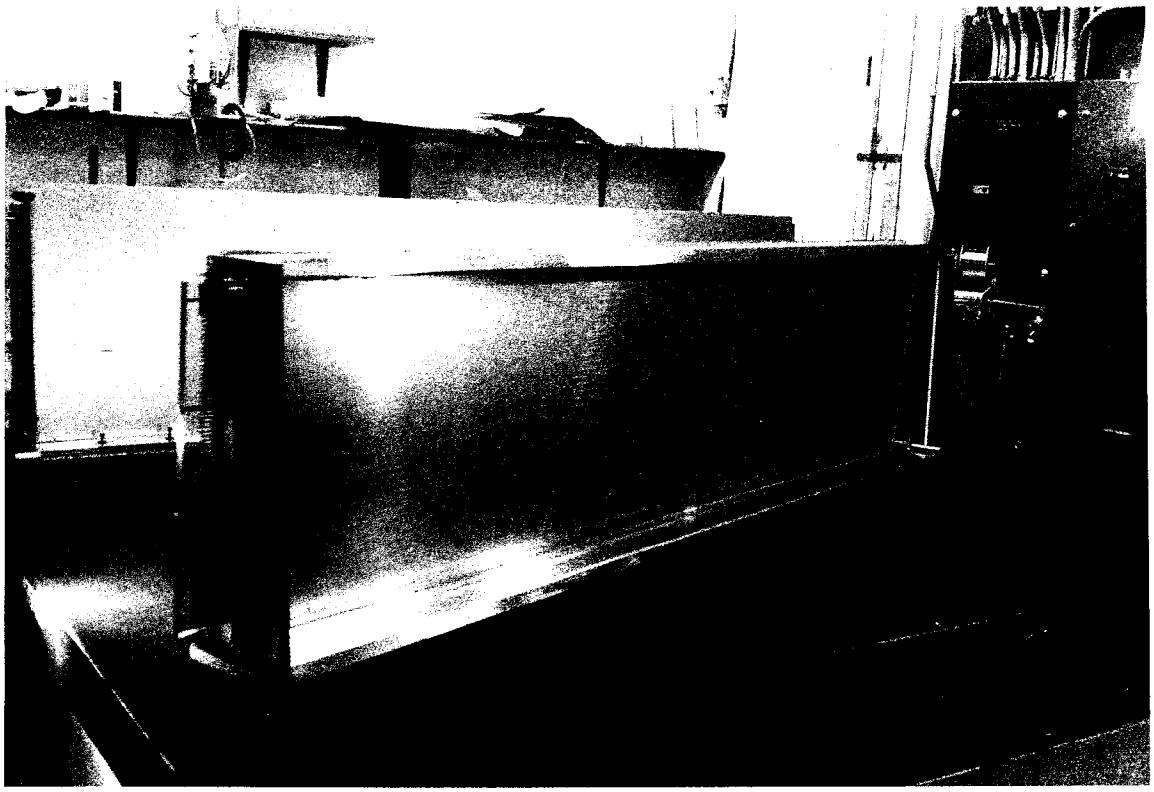

2-82 4260A16

Fig. 4

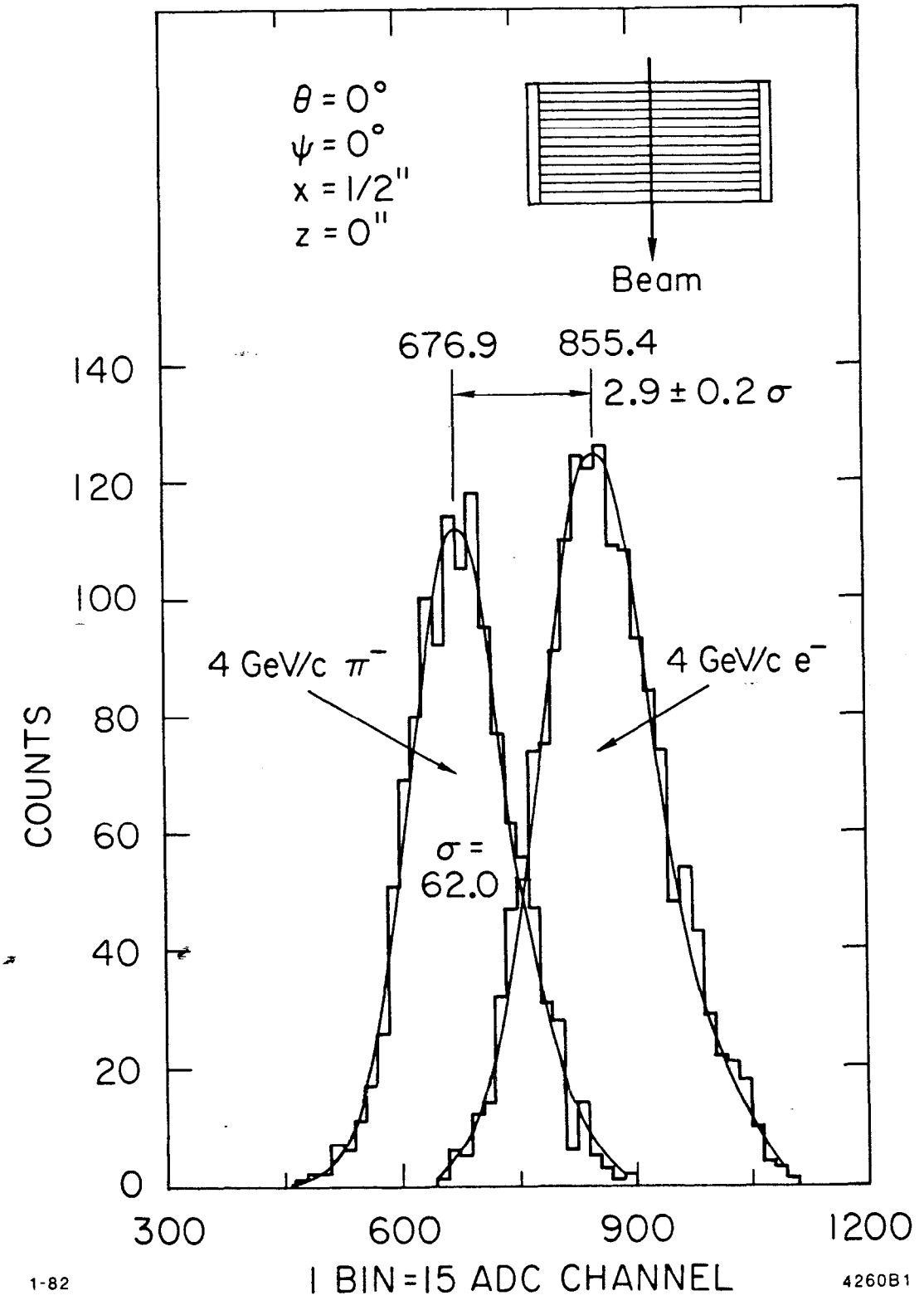
θ = 0°
ψ = 0°
x = 1/2"
z = 0"
Beam
676.9
855.4
2.9 ± 0.2 σ
140
120
100
80
60
40
20
0
COUNTS
4 GeV/c π⁻
4 GeV/c e⁻
σ = 62.0
300
600
900
1200
1 BIN = 15 ADC CHANNEL
1-82
4260B1

Fig. 5

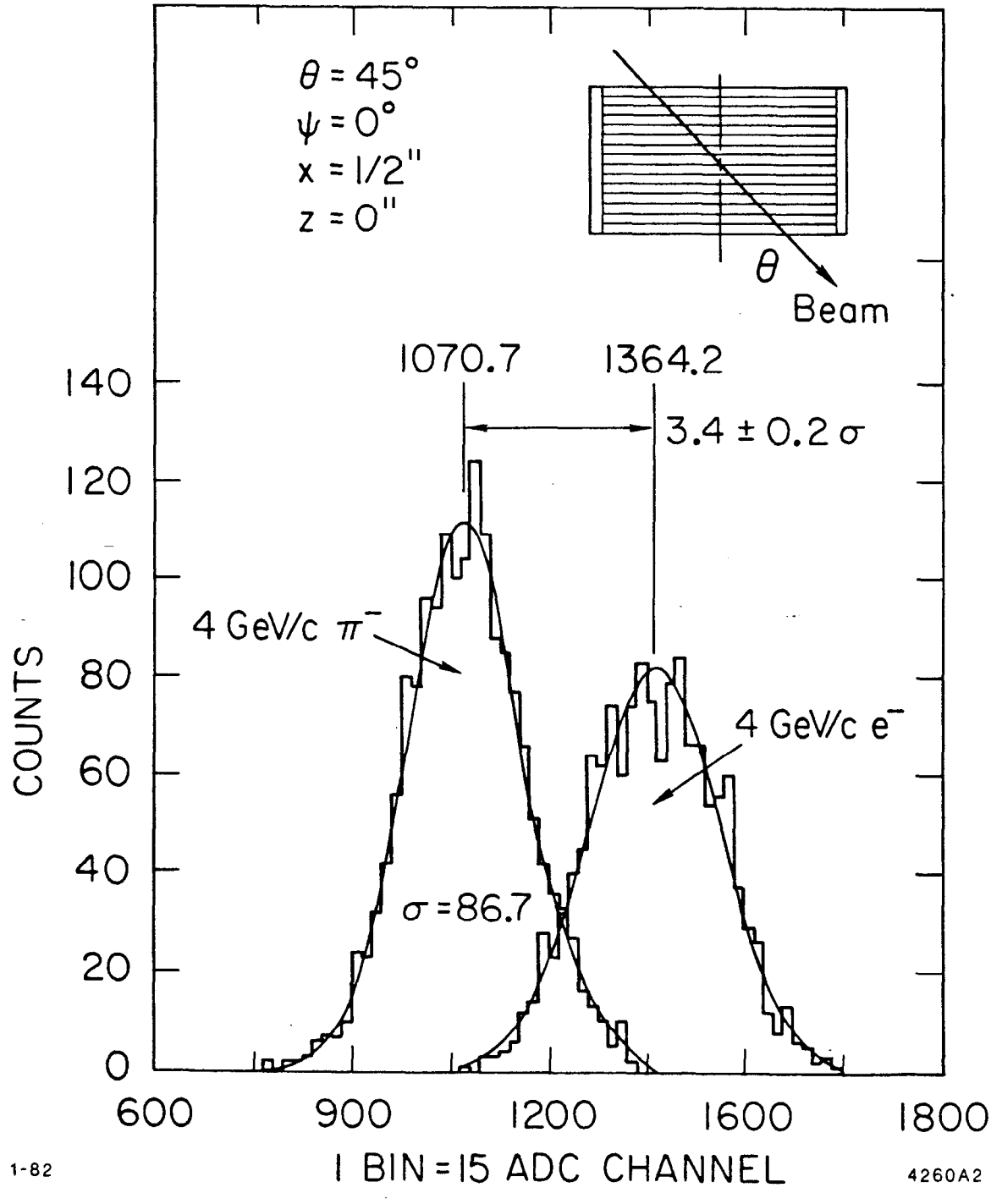
θ = 45°
ψ = 0°
x = 1/2"
z = 0"
θ
Beam
1070.7
1364.2
3.4 ± 0.2 σ
4 GeV/c π⁻
4 GeV/c e⁻
σ = 86.7
COUNTS
140
120
100
80
60
40
20
0
600
900
1200
1600
1800
1 BIN = 15 ADC CHANNEL
1-82
4260A2

Fig. 6

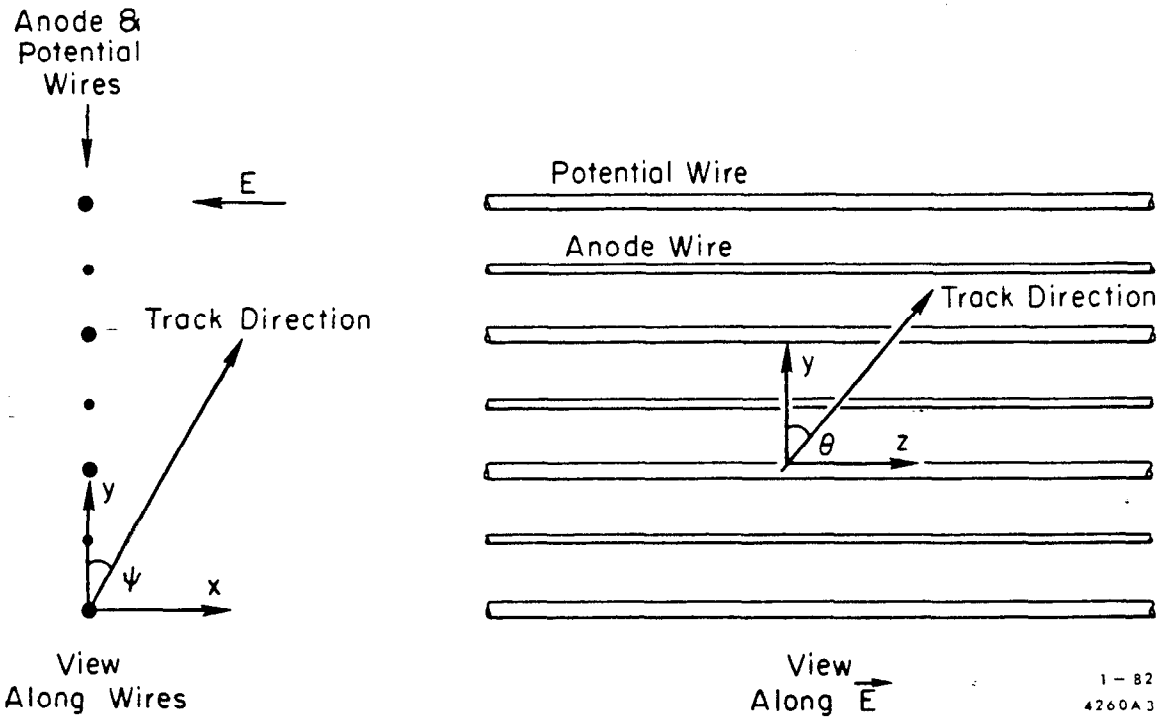
Anode &
Potential
Wires
E
Track Direction
y
ψ
x
View
Along Wires
Potential Wire
Anode Wire
Track Direction
y
θ
z
View
Along E
1 – 82
4260A3

Fig. 7

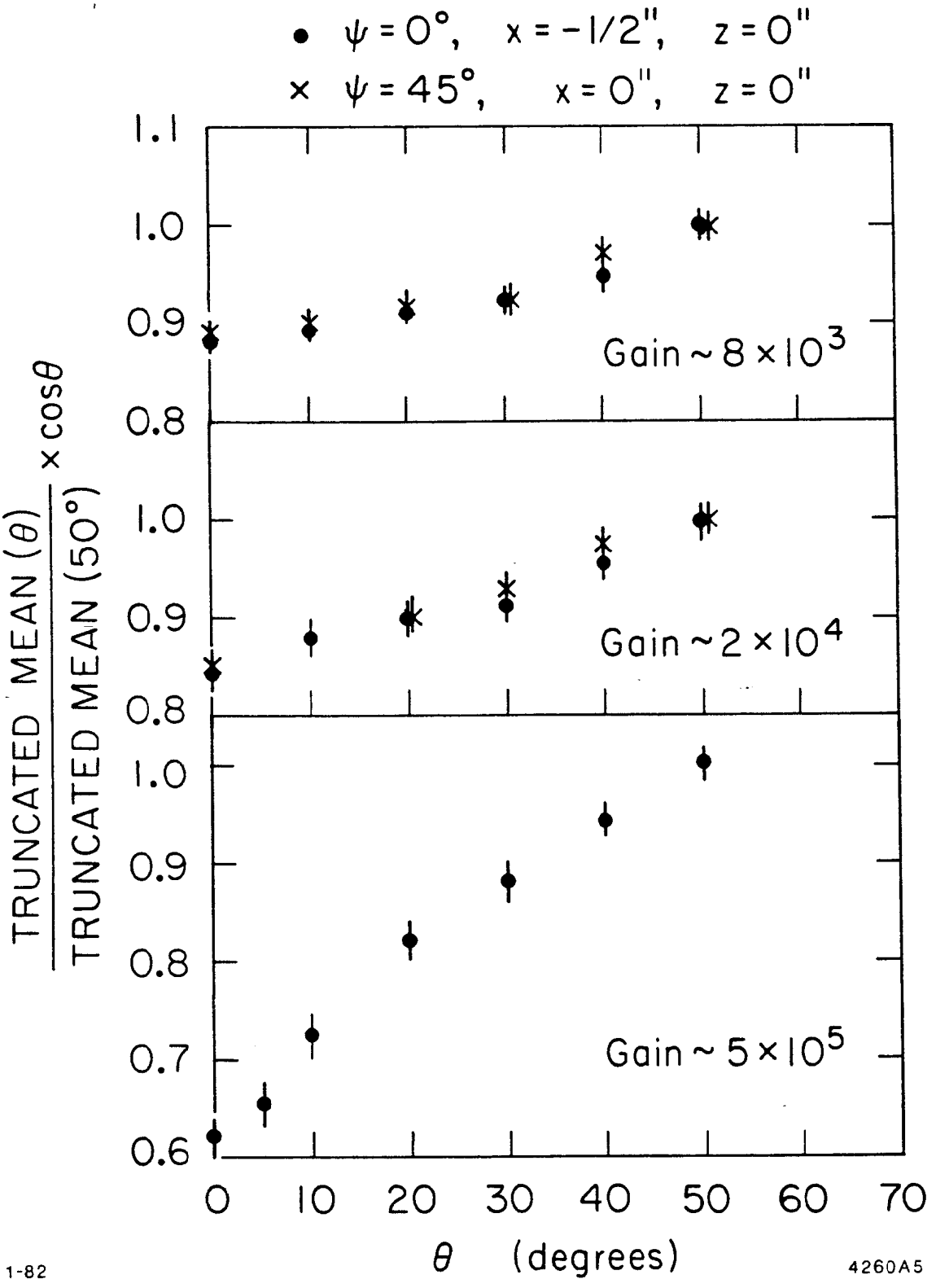
● ψ = 0°, x = −1/2", z = 0"
× ψ = 45°, x = 0", z = 0"
Gain ~ 8 × 10^3
Gain ~ 2 × 10^4
Gain ~ 5 × 10^5
TRUNCATED MEAN (θ) / TRUNCATED MEAN (50°) × cosθ
θ (degrees)
1.1
1.0
0.9
0.8
0.7
0.6
0
10
20
30
40
50
60
70
1-82
4260A5

Fig. 8

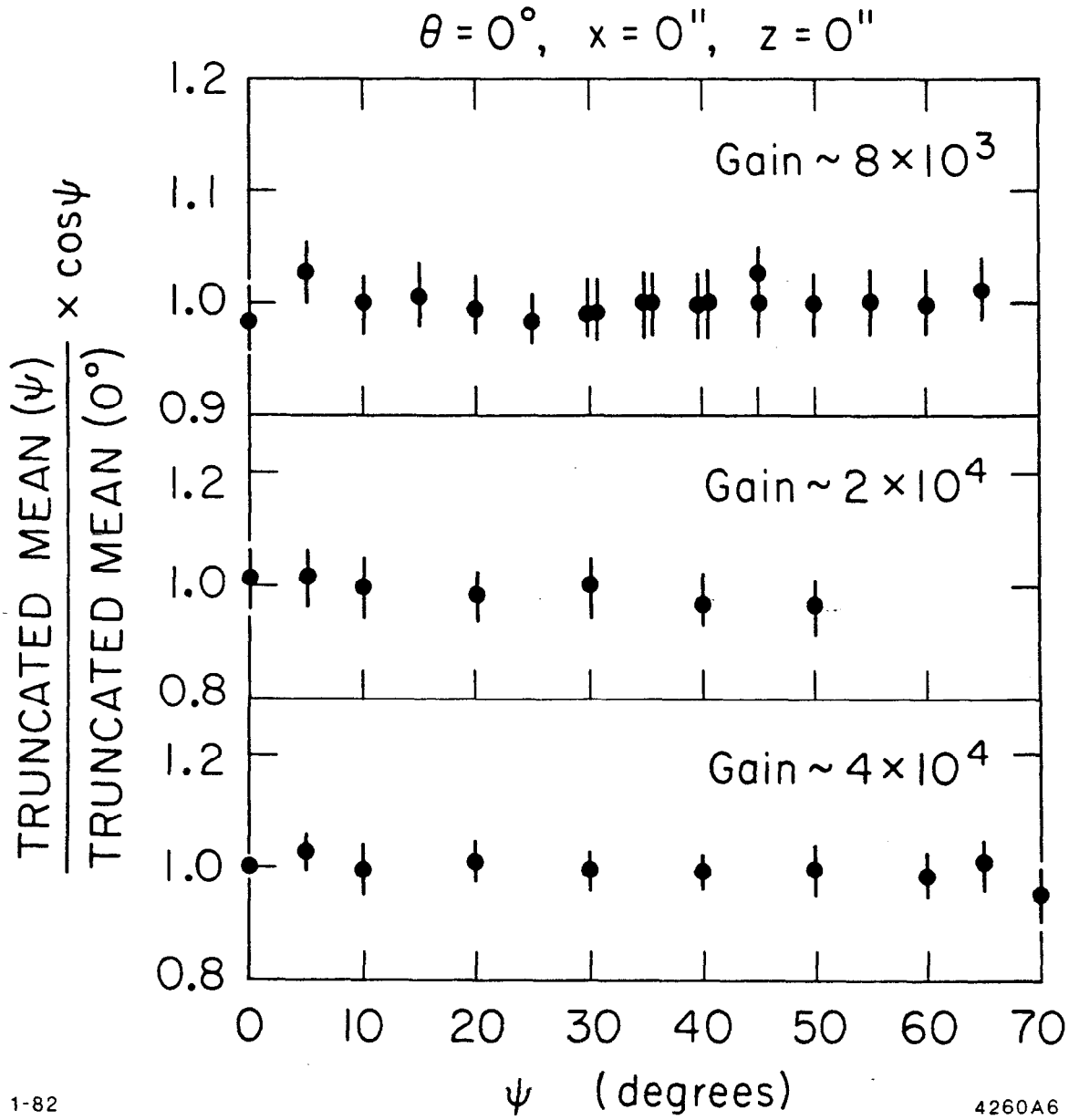
θ = 0°, x = 0", z = 0"
Gain ~ 8×10^3
Gain ~ 2×10^4
Gain ~ 4×10^4
TRUNCATED MEAN (ψ) / TRUNCATED MEAN (0°) × cosψ
ψ (degrees)
1.2
1.1
1.0
0.9
0.8
0
10
20
30
40
50
60
70
1-82
4260A6

Fig. 9

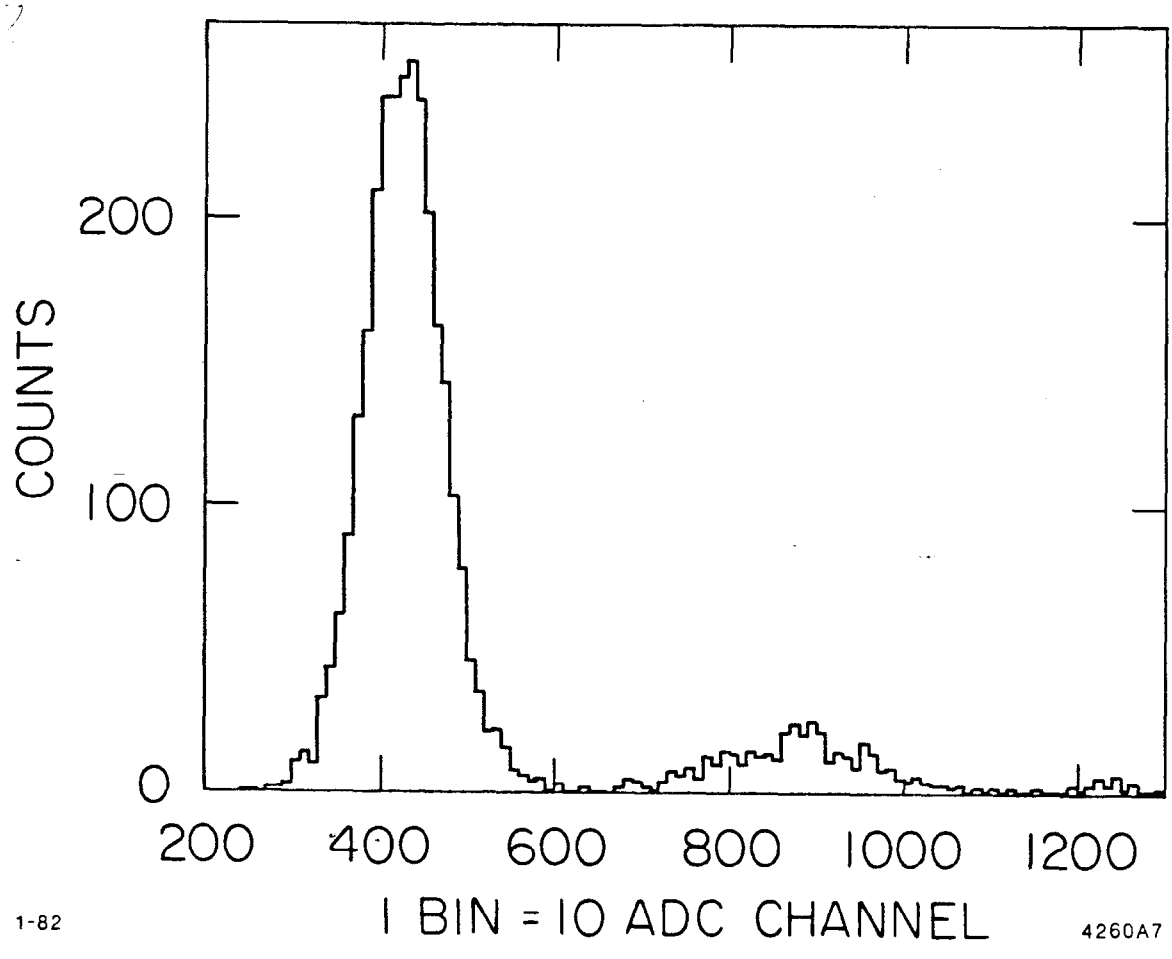
COUNTS
200
100
0
200
400
600
800
1000
1200
1 BIN = 10 ADC CHANNEL
1-82
4260A7

Fig. 10

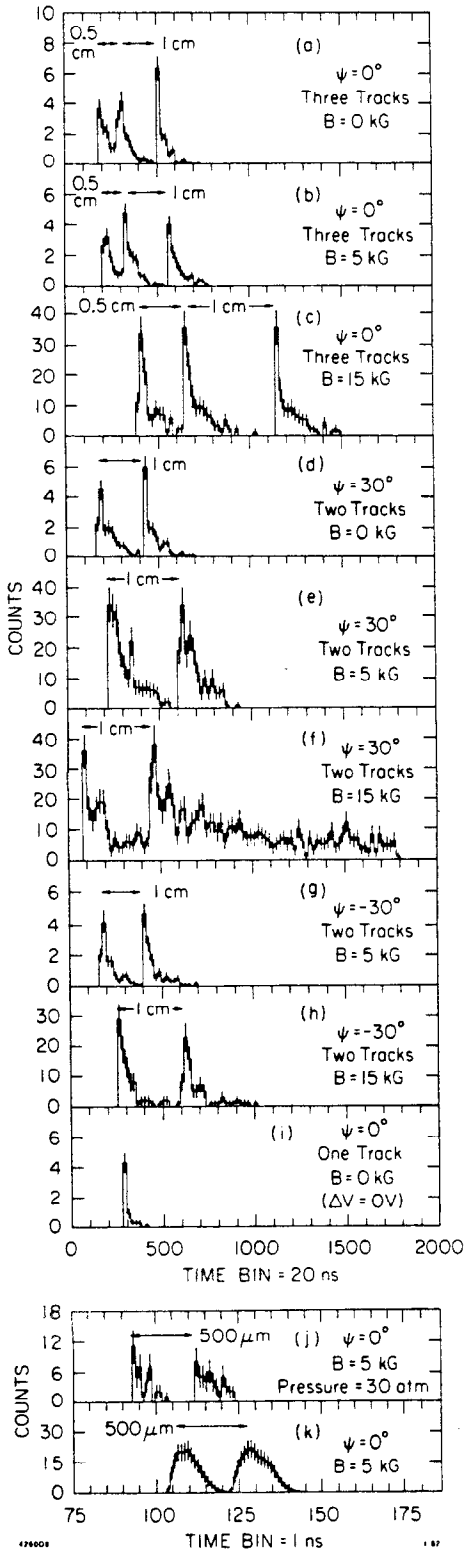
0.5 cm
1 cm
(a)
ψ = 0°
Three Tracks
B = 0 kG
(b)
ψ = 0°
Three Tracks
B = 5 kG
(c)
ψ = 0°
Three Tracks
B = 15 kG
(d)
ψ = 30°
Two Tracks
B = 0 kG
(e)
ψ = 30°
Two Tracks
B = 5 kG
(f)
ψ = 30°
Two Tracks
B = 15 kG
(g)
ψ = -30°
Two Tracks
B = 5 kG
(h)
ψ = -30°
Two Tracks
B = 15 kG
(i)
ψ = 0°
One Track
B = 0 kG
(ΔV = 0V)
COUNTS
TIME BIN = 20 ns
500 μm
(j)
ψ = 0°
B = 5 kG
Pressure = 30 atm
(k)
ψ = 0°
B = 5 kG
COUNTS
TIME BIN = 1 ns

Fig. 11

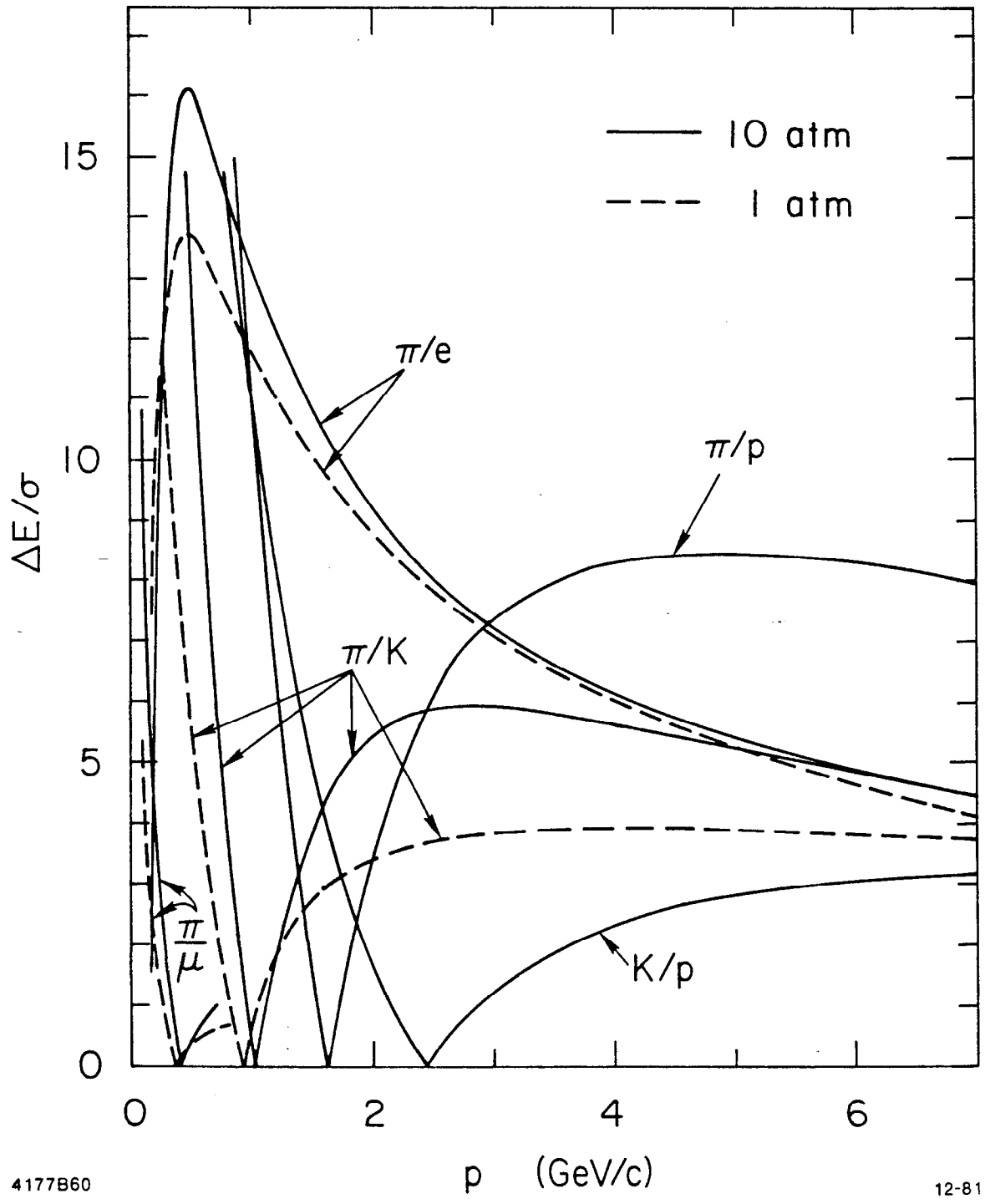

Fig. 12

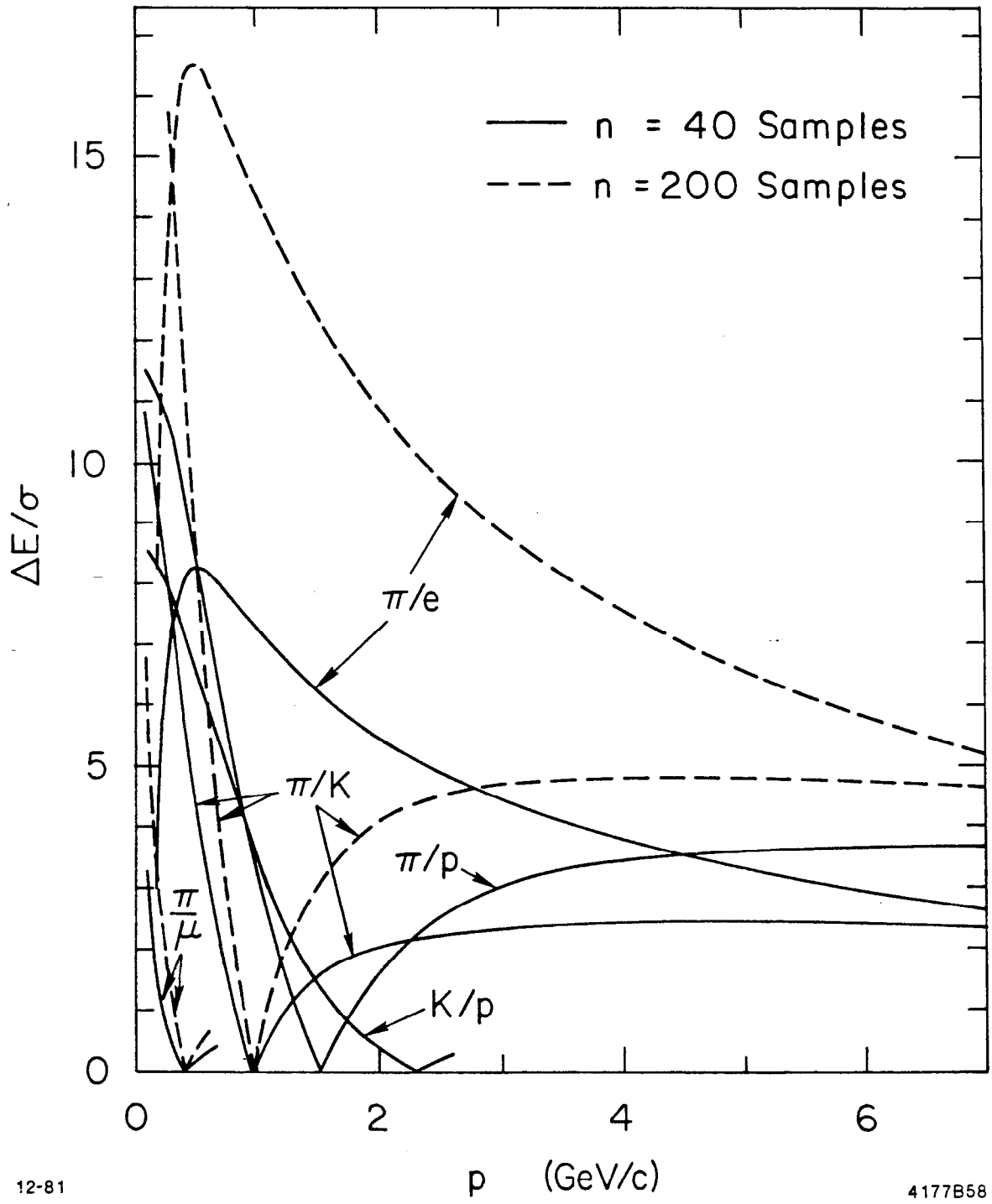
n = 40 Samples
n = 200 Samples
15
10
5
0
ΔE/σ
π/e
π/K
π/p
π/μ
K/p
0
2
4
6
p (GeV/c)
12-81
4177B58

Fig. 13

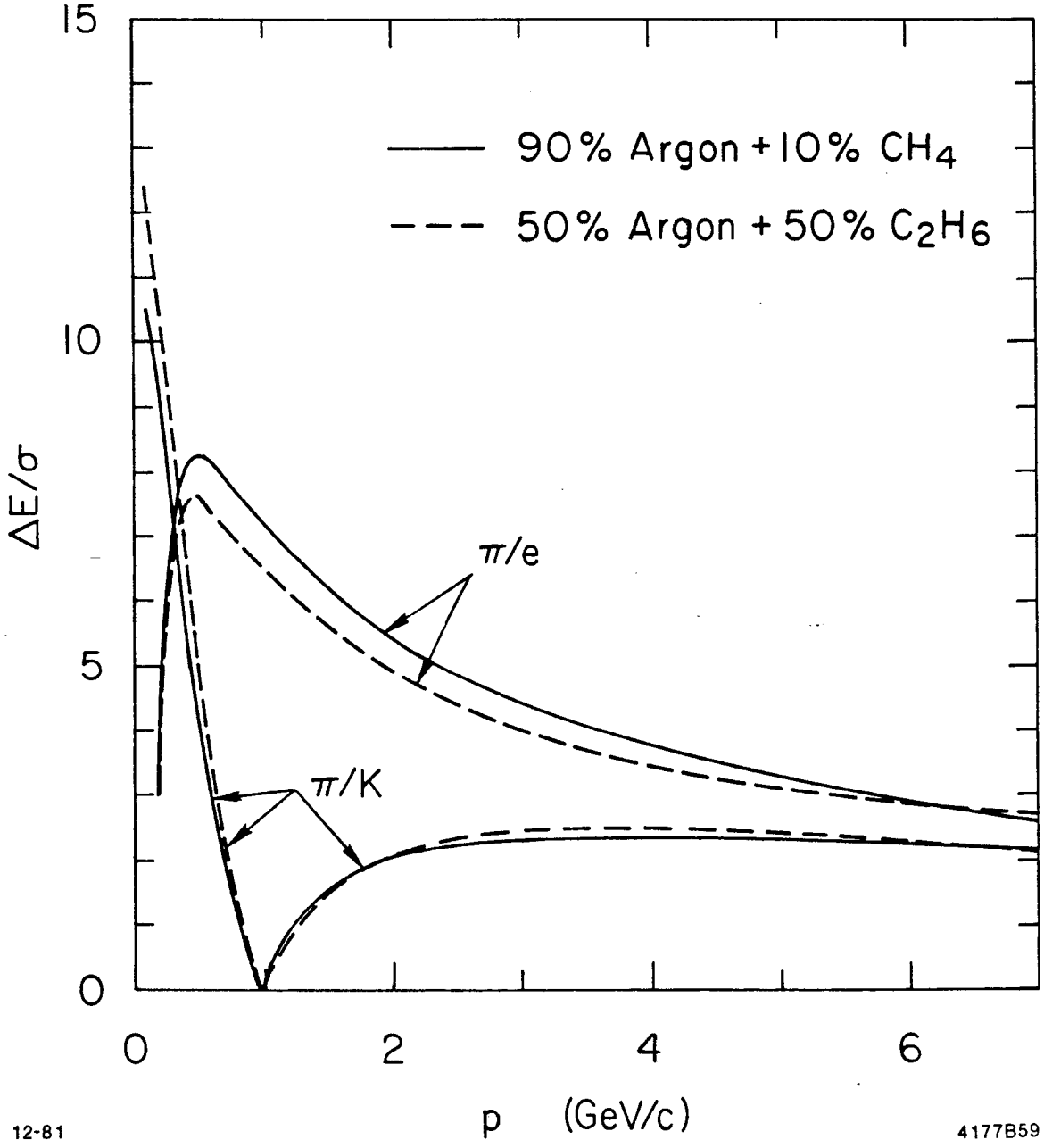
15
10
5
0
ΔE/σ
90% Argon + 10% CH4
50% Argon + 50% C2H6
π/e
π/K
0
2
4
6
p (GeV/c)
12-81
4177B59

Fig. 14